DOI: 10.1002/cctc.201100051

Catalytic Alkylation Routes via Carbonium-Ion-Like Transition States on Acidic Zeolites

Rajamani Gounder[a] and Enrique Iglesia*[a, b]

Brønsted acid sites in zeolites catalyze alkene hydrogenation with H_2 via the same kinetically-relevant $(C\text{-}H\text{-}H)^+$ carbonium-ion-like transition states as those involved in monomolecular alkane dehydrogenation.[1] Reactions between C_3H_6 and H_2 selectively form C_3H_8 (>80% carbon basis) at high H_2/C_3H_6 ratios (>2500) and temperatures (>700 K).[1] Ratios of C_3H_8 dehydrogenation to C_3H_6 hydrogenation rate constants (718–778 K) were identical on H-FER, H-MFI, and H-MOR zeolites and equal to the equilibrium constant for the stoichiometric gas-phase reaction, consistent with De Donder non-equilibrium thermodynamic treatments of chemical reaction rates.[2,3] The seemingly fortuitous extensions of the principle of microscopic reversibility[4] and the De Donder relations beyond their rigorous descriptions of chemical reaction dynamics at equilibrium and far from equilibrium but at identical (T, P_j), respectively, reflect the persistence of the same single kinetically-relevant step and the prevalence of unoccupied H^+ sites at the different conditions used to measure forward and reverse rates.[1]

By inference, larger alkanes should also form in direct alkene-alkane addition steps via the same $(C\text{-}C\text{-}H)^+$ *carbonium-ion-like transition states* involved in monomolecular alkane cracking. These chemical processes differ from alkylation mechanisms prevalent on liquid and solid acids (e.g., HF, H_2SO_4, H-zeolites) and superacids (e.g., $HF\text{-}SbF_5$, $HF\text{-}TaF_5$), which are mediated by *carbenium-ion chain carriers* that terminate as alkanes via hydride transfer.[5] Carbonium-ions contain three-atom/two-electron centers[6,7] and have been posited to mediate the formation of C_3H_8 in reactions of $CH_4\text{-}C_2H_4$ mixtures on superacids at the low temperatures (<573 K) required for favorable alkylation thermodynamics.[8–11] Here, we provide definitive kinetic and isotopic evidence that catalytic $CH_4\text{-}C_2H_4$ alkylation reactions are mediated by the same transition states involved in monomolecular alkane cracking, even on zeolitic Brønsted acid sites at high temperatures (>700 K).

Monomolecular alkane cracking routes prevail at high temperatures and low concentrations of alkene products; they involve late $(C\text{-}C\text{-}H)^+$ carbonium-ion-like transition states in kinetically-relevant C–C bond cleavage steps and unoccupied H^+ sites as most abundant surface intermediates (MASI).[6,7,12–16] Minority species adsorbed on H^+ sites are in quasi-equilibrium with gas phase reactants and products, leading to monomolecular C_3H_8 cracking rates given by Equation (1):

$$\vec{r}_c = K_1 k_2 P_{C_3H_8} = k_{meas,c} P_{C_3H_8} \quad (1)$$

Here, K_1 is the equilibrium constant for intrazeolite C_3H_8 adsorption and k_2 is the rate constant for the elementary step that forms $C_2H_5{}^+Z^-$ and CH_4 via $(C_3H_9)^+$ transition states (Scheme 1). Measured monomolecular cracking rate constants

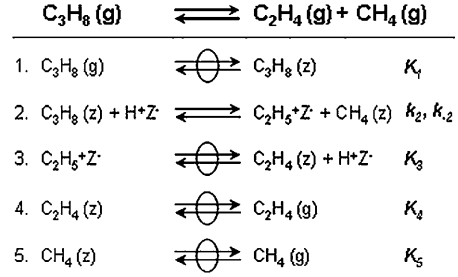

Scheme 1. Catalytic cycle for monomolecular C_3H_8 cracking and $CH_4\text{-}C_2H_4$ alkylation on Brønsted acid sites (H^+Z^-) within zeolites. Species are in the gas phase (g), chemically-bound to oxygen atoms at framework Al sites (Z^-), and physisorbed within zeolite channels near acid sites (z). Stoichiometric numbers (σ) are shown for each elementary step.

($k_{meas,c}$) reflect free energy differences between these transition states, stabilized within zeolite voids, and reactants in the gas phase (derivation and data in Section S.1 in the Supporting Information). As a result, rates are influenced by solvation effects that depend on spatial constraints characteristic of specific zeolite structures (Table 1; FER, MFI, MOR).[16]

Rates of the reverse reaction, in which CH_4 and C_2H_4 react to form C_3H_8, were first-order in CH_4 and C_2H_4 pressures (Figure 1;

Table 1. Rate constants for monomolecular C_3H_8 cracking ($k_{meas,c}$), $CH_4\text{-}C_2H_4$ alkylation ($k_{meas,alk}$) and C_2H_4 dimerization ($k_{meas,dim}$), and rate constant ratios on H-zeolites at 748 K.

Zeolite	$k_{meas,c}$ ($\times 10^3$)[a]	$k_{meas,alk}$ ($\times 10^4$)[b]	$k_{meas,dim}$[c]	$k_{meas,c}/k_{meas,alk}$ [bar]	$k_{meas,alk}$ ($\times 10^4$)/ $k_{meas,dim}$
FER	6.4	2.1	0.48	31 ± 6	4.3 ± 0.9
MFI	9.2	3.8	0.99	24 ± 5	3.8 ± 0.8
MOR-56	1.4	0.55	0.63	26 ± 5	1.2 ± 0.2

[a] mol (mol H^+)$^{-1}$ s^{-1} (bar C_3H_8)$^{-1}$. [b] mol (mol H^+)$^{-1}$ s^{-1} (bar C_2H_4)$^{-1}$ (bar CH_4)$^{-1}$. [c] mol (mol H^+)$^{-1}$ s^{-1} (bar C_2H_4)$^{-2}$.

[a] *R. Gounder, Prof. E. Iglesia*
Department of Chemical Engineering
University of California at Berkeley
Berkeley, CA 94720 (USA)
Fax: (+1) 510-642-4778
E-mail: iglesia@berkeley.edu
Homepage: http://iglesia.cchem.berkeley.edu/

[b] *Prof. E. Iglesia*
Division of Chemical Sciences
E.O. Lawrence Berkeley National Laboratory
Berkeley, CA 94720 (USA)

Supporting information for this article is available on the WWW under http://dx.doi.org/10.1002/cctc.201100051.

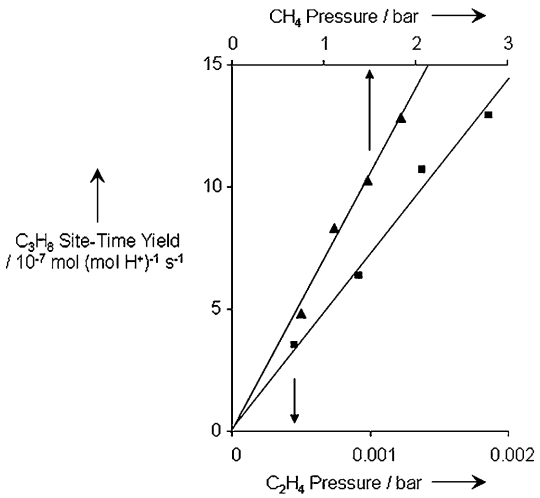

Figure 1. Dependence of C_3H_8 synthesis rates (748 K) on C_2H_4 pressure (■; $P(CH_4) = 1.8$ bar) and CH_4 pressure (▲; $P(C_2H_4) = 0.002$ bar) on H-MFI.

748 K; H-MFI) on all zeolites (data in Section S.2); no conversion was detected with CH_4 as the sole reactant. This kinetic behavior is consistent with Scheme 1 when steps 3–5 are quasi-equilibrated and H^+ sites are the MASI [Eq. (2)]:

$$\bar{r}_{alk} = k_{-2}K_3^{-1}K_4^{-1}K_5^{-1}P_{C_2H_4}P_{CH_4} = k_{meas,alk}P_{C_2H_4}P_{CH_4} \quad (2)$$

Here, k_{-2} is the rate constant for the formation of C_3H_8 via $(C_3H_9)^+$ transition states and K_3, K_4, and K_5 are the equilibrium constants that relate intrazeolite CH_4, C_2H_4, and $C_2H_5{}^+Z^-$ concentrations to CH_4 and C_2H_4 pressures. As for cracking ($k_{meas,c}$), measured rate constants for alkylation ($k_{meas,alk}$) depend on zeolite structure (Table 1), which stabilizes transition states, but not gaseous reactants (derivation and data in Section S.2). The $k_{meas,c}/k_{meas,alk}$ ratios, however, were the same (within experimental error) on H-FER, H-MFI, and H-MOR-56 [24–31 bar (1 bar = 0.1 MPa); 748 K; Table 1] and were equal to the equilibrium constant for the gas-phase reaction in Scheme 1 (K_{R1} = 26 bar; 748 K; calculation in Section S.3).

Rate constants in forward ($\overrightarrow{k}$) and reverse ($\overleftarrow{k}$) directions of a single-path catalytic sequence, at the same thermodynamic activities of all species [i.e. fixed (T, P_j)], are related to the equilibrium constant for the overall reaction (K_R) and the affinity-averaged stoichiometric number ($\bar{\sigma} = 1$ in Scheme 1) by De Donder relations [Eq. (3)]:[3]

$$\vec{k}\Big/\overleftarrow{k} = K_R^{1\sqrt{\sigma}} \quad (3)$$

The strict adherence of $\overrightarrow{k}$ and $\overleftarrow{k}$ to Equation (3) when the two parameters are measured at *different conditions* (T, P_j), however, is not required unless the same single elementary step (Step 2, Scheme 1) is kinetically-relevant in both directions and the active sites (H^+) are predominantly unoccupied at the different reaction conditions (derivation in Section S.4).[1] Thus, the agreement between $k_{meas,c}/k_{meas,alk}$ ratios among all samples (Table 1) and their numerical equivalence with K_{R1} indicate that the same kinetically-relevant $(C\text{-}C\text{-}H)^+$ transition state (Step 2, Scheme 1) mediates monomolecular alkane cracking and alkane–alkene alkylation reactions, even though the reactant configurations required to form this transition state are quite different in the two directions. In turn, the cations formed incipiently in either direction differ in structure and orientation, but they must access the same transition state through kinetically-insignificant conformational changes to give transition state free energies (reflected in $k_{meas,c}$ and $k_{meas,alk}$) that are measured with respect to gaseous reactants. These effects are consistent with the facile rotation of cationic species formed during acid-catalyzed hydrocarbon reactions, as shown by theoretical studies[17] and as found for alkane dehydrogenation-alkene hydrogenation.[1]

Propane formation through paths other than that in Scheme 1 (e.g., H-transfer between CH_4 and propoxides formed from C_2H_4 oligomerization-cracking cycles) may also occur at rates proportional to CH_4 pressure, but would require an implausible coincidence of rate constants for monomolecular C_3H_8 cracking and the mechanistically-unrelated step so as to give ratios equal to the C_3H_8 cracking equilibrium constant. These alternate paths are also ruled out by the isotopologues formed in $^{13}CH_4$-$^{12}C_2H_4$ reactions (Table 2; H-MFI; 748 K). C_3H_8 molecules predominantly contain one ^{13}C-atom (91%) and the

Table 2. Product isotopologues formed from $^{13}CH_4$-$^{12}C_2H_4$ reactions on H-MFI at 748 K.

Product	Mole fraction			
	0 ^{13}C	1 ^{13}C	2 ^{13}C	3 ^{13}C
C_3H_8	0.09	0.91	0	0
C_3H_6	0.88	0.12	0	0

C_3H_6 molecules formed are predominantly unlabeled (88%) and reflect oligomerization-cracking reactions of $^{12}C_2H_4$. These isotopologue distributions, taken together with the linear dependence of C_3H_8 synthesis rates on CH_4 and C_2H_4 pressures and the agreement between $k_{meas,c}/k_{meas,alk}$ ratios and K_{R1} [Table 1, Eq. (3)] constitute clear and rigorous evidence for direct CH_4-C_2H_4 alkylation via carbonium-ion-like transition states.

Reactions of CH_4-C_2H_4 mixtures on acidic zeolites form C_3H_8 as the predominant product only at high CH_4/C_2H_4 ratios (> 3000; Figure 2); C_3, C_4, and C_6 alkenes are also formed (Figure 2), but with a total selectivity that decreases with increasing CH_4/C_2H_4 ratios (data in Section S.2). These trends reflect competitive reactions of ethoxides (Scheme 2) with CH_4 (alkylation to form C_3H_8) and C_2H_4 (dimerization to form butoxides), consistent with products of C_2H_4 reactions on H-zeolites in the absence of CH_4 that reflect solely the latter route (data in Section S.5). The butoxides formed from C_2H_4 dimerization can desorb as butene isomers or react further with C_2H_4 to form larger C_6 oligomers, which desorb as alkenes, isomerize, undergo β-scission to form predominantly C_3H_6[18–20] or cyclize to form arenes after hydrogen transfer.[21]

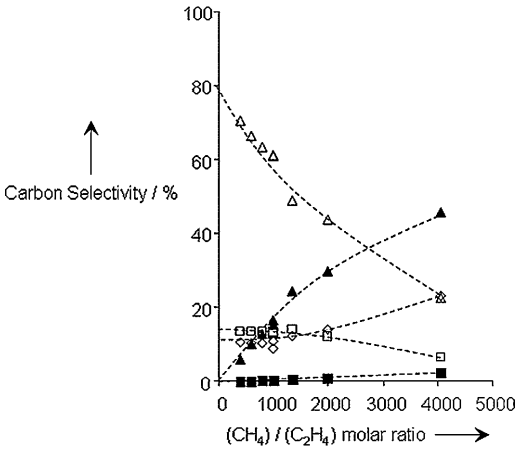

Figure 2. Carbon selectivity to C_3H_8 (▲), *n*-C_4H_{10} (■), C_3H_6 (△), C_4H_8 (□), and unsaturated C_6 (◇) products formed during CH_4-C_2H_4 reactions on H-MFI at 748 K with varying CH_4/C_2H_4 molar ratio. Dashed curves are included to guide the eye.

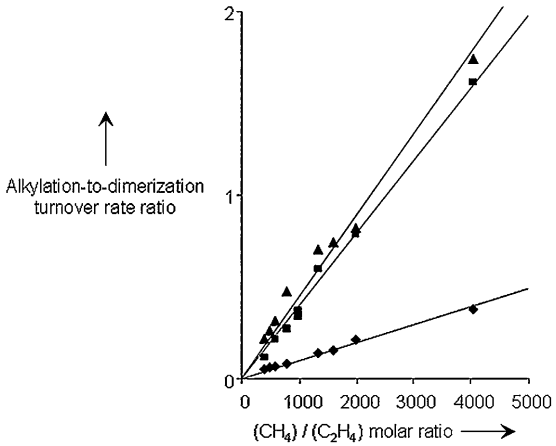

Figure 3. Alkylation-to-dimerization turnover rate ratios (748 K) with varying CH_4/C_2H_4 molar ratio on H-FER (▲), H-MFI (■), and H-MOR-56 (◆).

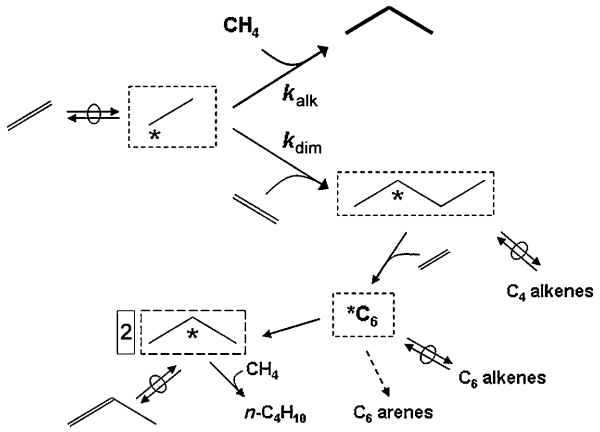

Scheme 2. Reaction scheme for CH_4-C_2H_4 alkylation (k_{alk}) and C_2H_4 dimerization (k_{dim}) on acidic zeolites. Surface intermediates (denoted by an asterisk, enclosed in dashed boxes) of a given carbon number are present as quasi-equilibrated alkoxides, carbenium ions, and physisorbed alkenes; we refer to these as alkoxides for ease of discussion.

The rates of formation of unsaturated C_3–C_6 species are related to the rate at which C_4 intermediates ($C_4H_9^+Z^-$) are formed (Scheme 2) by Equation (4):

$$r_{dim} = r_{C_4H_9^+Z^-} = r_{C_4H_8} + \sum r_{C_6} + \frac{1}{2}\left(r_{C_3H_6} + r_{C_4H_{10}}\right) \quad (4)$$

When H^+ sites are the MASI, C_2H_4 dimerization rates are second-order in C_2H_4 pressure (derivation in Section S.5) and alkylation-to-dimerization rate ratios are given by Equation (5):

$$r_{alk}/r_{dim} = \left(k_{meas,alk}/k_{meas,dim}\right)\left(P_{CH_4}/P_{C_2H_4}\right) \quad (5)$$

This is consistent with r_{alk}/r_{dim} ratios that are strictly proportional to CH_4/C_2H_4 reactant ratios on H-FER, H-MFI, and H-MOR-56 (Figure 3). On all samples, rate constants for dimerization are 2000–12 000 times larger than for alkylation (Table 1; 748 K), reflecting the more effective stabilization of positively-charged transition state fragments (C_2 carbenium-ions) by alkenes in dimerization steps (C_2H_4) than alkanes in alkylation steps (CH_4).[17] Thus, selective alkylation to form C_3H_8 (>90%) would require very high CH_4/C_2H_4 ratios (>25 000) to offset the strong kinetic preference for C_2H_4 dimerization.

Rate constants for C_2H_4 dimerization steps can also be used to predict rate constants for the reverse reaction, monomolecular C_4H_8 cracking, from the gas-phase equilibrium constant (K_{R2} = 5.4 bar^{-1}; 748 K) and Equation (3). Indeed, predicted values on all samples are similar to measured C_4H_8 cracking rate constants (Figure 4), despite the different conditions (T, P_j) used to measure forward and reverse rates (details in Section S.6). These data provide yet another demonstration for the applicability of the De Donder relations beyond their intended bounds and even in cases where the observed kinetic behavior reflects complex chemical reaction networks involving multiple elementary steps (e.g., alkene oligomerization).

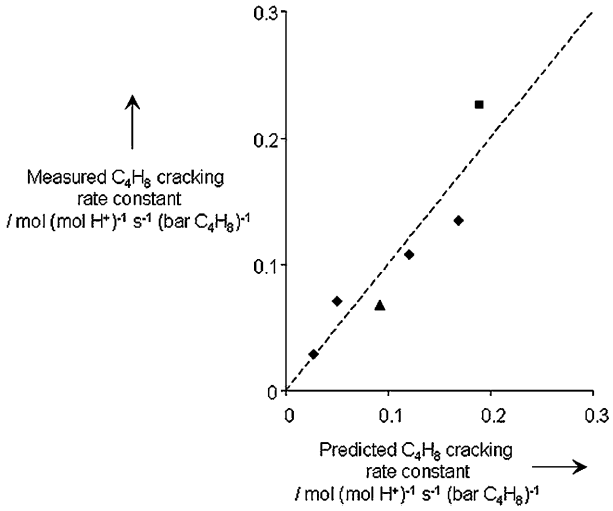

Figure 4. Monomolecular C_4H_8 cracking rate constants measured experimentally and predicted using C_2H_4 dimerization rate constants ($k_{meas,dim}$; Table 1 and Equation (3) on H-FER (▲), H-MFI (■), and MOR (◆) zeolites. Parity line is indicated by the dashed line.

Alkylation and dimerization transition states are expected to be stabilized differently by specific spatial constraints,[22] thus providing a potential strategy to influence selectivity, as found for alkane (C_3H_8, *n*-C_4H_{10}, *i*-C_4H_{10}) cracking and dehydrogenation paths by varying the distribution of H^+ between 8-MR side pockets and 12-MR channels (0.10–0.80 fraction in 8-MR) in MOR zeolites.[16,23] Rate constants for C_2H_4 dimerization (per total H^+) increased and $k_{meas,alk}/k_{meas,dim}$ ratios decreased monotonically with increasing H^+ fraction within 8-MR pockets (Figure 5). These data indicate that the kinetic preference for 8-MR H^+ is stronger for C_2H_4 dimerization than CH_4-C_2H_4 alkylation, which we surmise reflects larger entropy differences, in

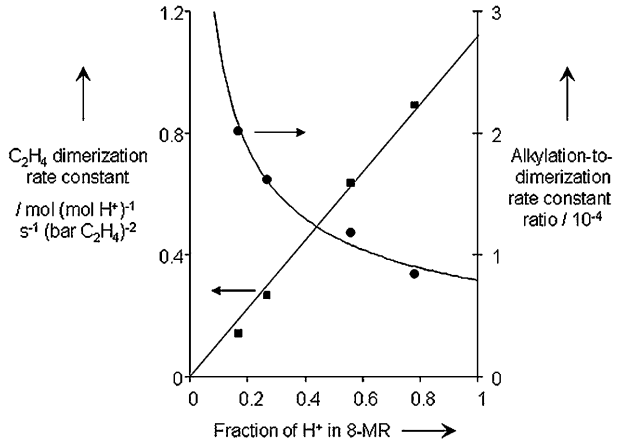

Figure 5. Dependence of C_2H_4 dimerization rate constants (■; $k_{meas,dim}$; per total H^+) and alkylation-to-dimerization rate constant ratios (●; $k_{meas,alk}/k_{meas,dim}$) at 748 K on the fraction of H^+ in 8-MR pockets of MOR zeolites.

the former reaction, between transition states confined partially within 8-MR pockets[16,23] and contained fully within 12-MR channels. The higher alkylation selectivity of 12-MR H^+ is accompanied by lower turnover rates for both alkylation and dimerization reactions.

These data show clearly that Brønsted acids catalyze alkane-alkene alkylation via the same $(C\text{-}C\text{-}H)^+$ carbonium-ion-like transition states required for monomolecular alkane cracking. Unfavorable thermodynamics (> 573 K) and alkene dimerization side reactions limit the useful practice of such routes, but alkylation selectivities can be increased by confining H^+ sites within structures that preferentially stabilize alkylation transition states. The De Donder relations apply even when reaction conditions differ, as long as the same single step limits rates and active sites remain predominantly unoccupied, enabling the prediction of rate constants in one direction of a catalytic sequence from thermodynamic data and rate constants in the other direction; such is the case for C_3H_8 cracking and CH_4-C_2H_4 alkylation, and for C_4H_8 cracking and C_2H_4 dimerization.

Experimental Section

MFI (Si/Al = 16.5, Zeolyst), FER (Si/Al = 10, Zeolyst) and MOR (Si/Al = 10, Zeolyst; Si/Al = 8.9, Tosoh) were obtained in the NH_4^+-form and converted to the H^+-form by treatment in flowing dry air (2.5 $cm^3 g^{-1} s^{-1}$, zero grade, Praxair) for 4 h at 773 K (0.0167 $K s^{-1}$). MOR samples are denoted by the percentage of H^+ in 8-MR pockets, determined by infrared deconvolution methods described together with all characterization data and Na^+-exchange protocols elsewhere.[16] Steady-state reaction rates were measured in a plug-flow tubular quartz reactor from product concentrations measured by gas chromatography and flame ionization detection (Agilent HP-6890GC).[16] CH_4 (99.97%), C_2H_4 (1% C_2H_4 (99.9%), 5% Ar, 94% He), C_3H_8 (10% C_3H_8 (99.999%), 5% Ar, 85% He), and C_4H_8 (1% 1-C_4H_8 (99.9%), 5% Ar, 94% He) reactants were obtained from Praxair. H-zeolites (0.08–0.50 g; 180–250 μm) were treated in flowing 5% O_2/95% He (16.7 $cm^3 g^{-1} s^{-1}$, 99.999%, Praxair) for 2 h at 803 K (0.0167 $K s^{-1}$) and then in He (16.7 $cm^3 g^{-1} s^{-1}$, 99.999%, Praxair) for 0.5 h at 748 K before reaction. Rate constants at the end of each experiment (≈ 12 h time-on-stream) were similar (within 5%) to initial values on all catalysts; thus, deactivation did not corrupt any kinetic data. Uncertainties are reported as 95% confidence intervals. Isotopic studies used $^{13}CH_4$ (99 atom% ^{13}C, Isotec) and $^{12}C_2H_4$ mixtures (80 kPa $^{13}CH_4$, 0.2 kPa $^{12}C_2H_4$) on H-MFI (0.05 g, 180–250 μm; 1.5×10^{-6} (mol carbon) $g^{-1} s^{-1}$) held within a tubular stainless steel reactor (4.6 mm i.d.) with a fritted VCR gasket and quartz wool. Temperatures were maintained by resistive heating (Watlow Series 96 controller) and measured with a K-type thermocouple. Products were measured by chromatography (HP-1 column, 50 m × 0.32 mm; 1.05 μm film; Agilent) using flame ionization and mass selective detectors (HP 5890/HP 5972). Mass spectra and matrix deconvolution methods[24] were used to measure isotopologue distributions.

Acknowledgements

We acknowledge the financial support from the Chevron Energy Technology Company.

Keywords: alkylation · Brønsted acid · carbonium ion · cracking · zeolites

[1] R. Gounder, E. Iglesia, *J. Catal.* **2011**, *277*, 36.
[2] a) T. de Donder, *L'Affinité*, Gauthier-Villars, Paris, **1927**; b) T. de Donder, P. van Rysselberghe, *Thermodynamic Theory of Affinity: A Book of Principles*, Stanford University Press, Stanford, **1936**.
[3] M. Boudart, G. Djéga-Mariadassou, *Kinetics of Heterogeneous Catalytic Reactions*, Princeton University Press, Princeton, **1984**.
[4] a) R. C. Tolman, *Phys. Rev.* **1924**, *23*, 693; b) R. C. Tolman, *Proc. Natl. Acad. Sci. USA* **1925**, *11*, 436.
[5] A. Corma, A. Martinez, *Catal. Rev. Sci. Eng.* **1993**, *35*, 483.
[6] J. A. Lercher, R. A. van Santen, H. Vinek, *Catal. Lett.* **1994**, *27*, 91.
[7] A. M. Rigby, G. J. Kramer, R. A. van Santen, *J. Catal.* **1997**, *170*, 1.
[8] G. A. Olah, J. D. Felberg, K. Lammertsma, *J. Am. Chem. Soc.* **1983**, *105*, 6529.
[9] M. Siskin, *J. Am. Chem. Soc.* **1976**, *98*, 5413.
[10] M. S. Scurrell, *Appl. Catal.* **1987**, *34*, 109.
[11] J. Sommer, M. Muller, K. Laali, *Nouv. J. Chim.* **1982**, *6*, 3.
[12] W. O. Haag, R. M. Dessau, *Proceedings - International Congress on Catalysis, 8th, Vol. 2*, Verlag Chemie, Weinheim, **1984**, p. 305.
[13] S. Kotrel, H. Knözinger, B. C. Gates, *Microporous Mesoporous Mater.* **2000**, *35–6*, 11.
[14] T. F. Narbeshuber, H. Vinek, J. A. Lercher, *J. Catal.* **1995**, *157*, 388.
[15] B. Xu, C. Sievers, S. B. Hong, R. Prins, J. A. van Bokhoven, *J. Catal.* **2006**, *244*, 163.
[16] R. Gounder, E. Iglesia, *J. Am. Chem. Soc.* **2009**, *131*, 1958.
[17] a) M. J. Janik, R. J. Davis, M. Neurock, *J. Catal.* **2006**, *244*, 65; b) M. J. Janik, R. J. Davis, M. Neurock, *Catal. Today* **2006**, *116*, 90.
[18] J. S. Buchanan, J. G. Santiesteban, W. O. Haag, *J. Catal.* **1996**, *158*, 279.

[19] J. Abbot, B. W. Wojciechowski, *Can. J. Chem. Eng.* **1985**, *63*, 462.
[20] a) T. Koyama, Y. Hayashi, H. Horie, S. Kawauchi, A. Matsumoto, Y. Iwase, Y. Sakamoto, A. Miyaji, K. Motokura, T. Baba, *Phys. Chem. Chem. Phys.* **2010**, *12*, 2541, see the Supporting Information.; b) K. Inazu, T. Koyama, A. Miyaji, T. Baba, *J. Jpn. Pet. Inst.* **2008**, *51*, 205.
[21] a) Y. V. Joshi, A. Bhan, K. T. Thomson, *J. Phys. Chem. B* **2004**, *108*, 971; b) A. Bhan, S. H. Hsu, G. Blau, J. M. Caruthers, V. Venkatasubramanian, W. N. Delgass, *J. Catal.* **2005**, *235*, 35; c) A. Bhan, W. N. Delgass, *Catal. Rev. Sci. Eng.* **2008**, *50*, 19.
[22] A. Bhan, E. Iglesia, *Acc. Chem. Res.* **2008**, *41*, 559.
[23] R. Gounder, E. Iglesia, *Angew. Chem.* **2010**, *122*, 820; *Angew. Chem. Int. Ed.* **2010**, *49*, 808.
[24] G. L. Price, E. Iglesia, *Ind. Eng. Chem. Res.* **1989**, *28*, 839.

Received: February 13, 2011
Published online on ■■ ■■, 0000

COMMUNICATIONS

*R. Gounder, E. Iglesia**

■■ – ■■

Catalytic Alkylation Routes via Carbonium-Ion-Like Transition States on Acidic Zeolites

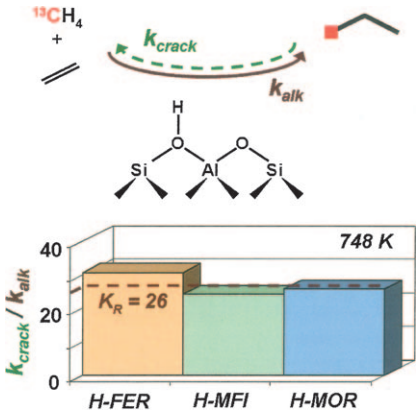

Zeolites going crackers: Brønsted acid sites in zeolites (H-FER, H-MFI, H-MOR) catalyze CH_4-alkene reactions at high temperatures (> 700 K) via carbonium-ion-like transition states. The ratio of rate constants for forward and reverse reactions (alkane alkylation-cracking, alkene dimerization-cracking) equal their respective equilibrium constants (K_R). In contrast, relative rates of CH_4 and alkene reactions with a given alkoxide are influenced by the local environment around acid sites.

